



Hydrogen Bond Properties and Dynamics of Liquid–Vapor Interfaces of Aqueous Methanol Solutions

Sandip Paul and Amalendu Chandra*

Department of Chemistry, Indian Institute of Technology, Kanpur, India 208016

Received April 13, 2005

Abstract: The hydrogen bonded structure and dynamics of liquid–vapor interfaces of aqueous methanol solutions of varying compositions are investigated by means of molecular dynamics simulations. The dynamical aspects of the interfaces are investigated in terms of the single-particle dynamical properties such as the relaxation of velocity autocorrelation and the translational diffusion coefficients along the perpendicular and parallel directions and the dipole orientational relaxation of the interfacial water and methanol molecules and also in terms of the relaxation of water–water, water–methanol, and methanol–methanol hydrogen bonds at interfaces at 298 K. The results of the interfacial dynamics are compared with those of the corresponding bulk phases. The inhomogeneous density, anisotropic orientational profiles, surface tension, and the pattern of hydrogen bonding are calculated in order to characterize the location, width, microscopic structure, and the thermodynamic aspects of the interfaces and to explore their effects on the interfacial dynamical properties of water and methanol molecules.

1. Introduction

A detailed knowledge of the molecular properties of liquid–vapor interfaces of molecular liquids is important in the understanding of equilibrium and dynamical aspects of various chemical processes that occur at such interfaces. The present paper deals with the equilibrium and dynamical behavior of liquid–vapor interfaces of aqueous methanol solutions of varying composition. Monohydroxyl alcohol–water mixtures are interesting not only because of their ubiquitous nature but also due to their importance as model systems. The amphiphilic nature of alcohol molecules makes them excellent probes for studying the structure of aqueous solutions since they strongly interact with water through hydrogen bonding. Also, depending on the size of their alkyl groups, the alcohol molecules perturb the water structure through hydrophobic hydration as well. The molecular structure of liquid water consists of a tetrahedral network of hydrogen bonds. X-ray and neutron diffraction studies of liquid methanol^{1,2} have shown that each methanol molecule engages in approximately two hydrogen bonds giving rise to a chainlike structure similar to that found in the solid state. The chainlike structure has also been found in recent first principles simulations of liquid methanol.³ When mixed with water, it has been found that the water–methanol mixtures

show many interesting nonideal behavior in terms of both their equilibrium and dynamical properties.^{4–12} Mixing of methanol with water causes structural changes in the liquid due to rather strong interactions of water with the alcohol molecules. Several simulations have been carried out on dilute solutions of methanol in water.^{13–16} In particular, we note the Monte Carlo study of Jorgensen and Madura¹³ who used a methanol potential¹⁶ with explicit methyl hydrogens to study the solvation and conformation of methanol in water. The preferred conformation of a methanol molecule in water was found to be staggered, and the water molecules were found to form a cage around the methyl group. Subsequently, experimental studies based on neutron diffraction and isotopic substitution provided a detailed description of the structure of a hydration shell around a methanol molecule.¹⁷ The water molecules were found to form a loose hydrogen bonded shell around the methanol at a carbon-to-water distance of ≈ 3.7 Å supporting the picture of cagelike hydration of methanol in aqueous solutions.

There have also been a number of simulation studies on water–methanol mixtures of higher methanol concentrations in bulk liquid phases.^{18–25} However, studies of liquid–vapor interfaces of water–methanol mixtures have received relatively less attention. Matsumoto et al.²⁶ studied the structural

and thermodynamical aspects of liquid–vapor interfaces of water–methanol mixtures for a wide range of concentrations by using molecular dynamics simulations. They reported that the outermost layer of the interface is saturated with methanol even at low bulk concentrations of methanol. They also found that the density of water is enhanced as compared to the bulk density just inside the adsorbed methyl layer. The work of Matsumoto et al.²⁶ involved nonpolarizable models for both water and methanol molecules. Very recently, polarizable models have also been employed to study the liquid–vapor interfaces of pure methanol²⁷ and also of water–methanol mixtures.²⁸ These studies provided information on the variation of dipole moment across the interfaces which otherwise could not be obtained by using nonpolarizable models.

The experimental studies of the molecular orientational behavior of liquid–vapor interfaces primarily involve the surface specific methods such as second harmonic generation (SHG) and sum frequency generation (SFG). These methods have been used to investigate molecular orientation at a wide variety of interfaces involving pure water or aqueous solutions^{29–45} including water–methanol mixtures.^{29–31} It was found that the orientational order of methanol molecules at the surface of water–methanol increases with a decrease of methanol concentration. Very recently, Rao and co-workers⁴⁶ investigated the surface composition of water–alcohol mixtures by a combination of molecular beam and mass spectroscopic measurements. In this study, which was the first direct experimental verification of surface enrichment, alcohols of varying chain length were considered including methanol. The surfaces were found to be enriched by alcohol as compared to the bulk liquid composition, and the extent of enrichment was found to depend on the chain length of the alcohol molecules. Even for the mixture of water with the shortest alcohol of methanol, the surfaces were found to be enriched by the alcohol molecules.

We note that all the existing theoretical and experimental studies on liquid–vapor interfaces of water–methanol mixtures deal with their structural and thermodynamical properties. The dynamical properties, both of single molecules and hydrogen bonded pairs, at the liquid–vapor interfaces of water–methanol mixtures have not yet been investigated. We note that, for water–methanol mixtures, the dynamics of the interfaces is expected to be intimately related to the structure and energetics of hydrogen bonds that are present at such interfaces. Thus, it would be worthwhile to make a detailed molecular-level investigation of the hydrogen bonding and dynamical properties of liquid–vapor interfaces of water–methanol mixtures. The present work makes a contribution toward this end.

In this work, we have carried out molecular dynamics simulations of liquid–vapor interfaces of water–methanol solutions at varying composition. Our main focus has been to calculate the hydrogen bond and dynamical properties such as the average number of hydrogen bonds per molecule in different regions, the lifetimes of hydrogen bonds, the relaxation of the perpendicular and parallel components of velocity autocorrelation function and diffusion, and also the relaxation of single-particle dipole orientational correlation

Table 1. Values of the Lennard-Jones and Electrostatic Interaction Potential Parameters of Water and Methanol

	atom/ion	σ (Å)	ϵ (kcal/mol)	charge (e) ^a
water (SPC/E model)	O	3.169	0.1554	−0.8476
	H			+0.4238
methanol (H1 model)	CH ₃	3.861	0.1823	+0.297
	O	3.083	0.1758	−0.728
	H			+0.431

^a e represents the magnitude of electronic charge.

function of the interfacial water and methanol molecules. The dynamical properties of the interfaces are compared with those of the bulk phases. In addition, we have also calculated the inhomogeneous density and orientational profiles, surface tension, and also the distribution of hydrogen bonds as the dynamical properties of the interfaces are intimately related to these equilibrium quantities. Also, the density profiles help us to characterize the location and thickness of the interfaces.

The outline of the present paper is as follows. The details of the simulations including the construction of the interfaces and their characterization in terms of density profiles are presented in section 2. Calculations of interfacial structures and surface tensions are described in section 3. In section 4, we have discussed the hydrogen bond patterns in the bulk liquid and at the interfaces, and section 5 deals with the simulation results of the single-particle dynamics at the interfaces. The results of hydrogen bond dynamics are presented in section 6, and our conclusions are briefly summarized in section 7.

2. Details of Models, Simulation Method, and Construction of the Interfaces

We have carried out molecular dynamics simulations of the liquid–vapor interface of water–methanol mixtures at 298 K. We have used the H1 model for methanol molecules.⁴⁷ In this model, the methanol molecules are modeled as rigid objects with three interaction sites for short-range Lennard-Jones and long-range Coulomb interactions. The methyl group is considered as a united atom with a single interaction site. The water molecules are characterized by the SPC/E potential.⁴⁸ In these models, the interaction between atomic sites of two different molecules is expressed as

$$u_{\alpha\beta}(r_{\alpha}, r_{\beta}) = 4\epsilon_{\alpha\beta} \left[\left(\frac{\sigma_{\alpha\beta}}{r_{\alpha\beta}} \right)^{12} - \left(\frac{\sigma_{\alpha\beta}}{r_{\alpha\beta}} \right)^6 \right] + \frac{q_{\alpha}q_{\beta}}{r_{\alpha\beta}} \quad (1)$$

where $r_{\alpha\beta}$ is the distance between the atomic sites α and β , and q_{α} is the charge of the α th atom. The Lennard-Jones parameters $\sigma_{\alpha\beta}$ and $\epsilon_{\alpha\beta}$ are obtained by using the combination rules $\sigma_{\alpha\beta} = (\sigma_{\alpha} + \sigma_{\beta})/2$ and $\epsilon_{\alpha\beta} = \sqrt{\epsilon_{\alpha}\epsilon_{\beta}}$. The values of the potential parameters q_{α} , σ_{α} , and ϵ_{α} for methanol and water are summarized in Table 1.

We first carried out a bulk simulation in a cubic box of 864 molecules, periodically replicated in all three dimensions. The box length L was adjusted in such a way that the pressure would be close to the atmospheric pressure at 298 K. After this bulk solution was properly equilibrated, two empty boxes of equal size were added on either side of the original simulation box along the z -direction, and this larger rectan-

gular box (of dimension $L \times L \times 3L$) was taken as the simulation box in the next phase of the simulation run, and the system was reequilibrated by imposing periodic boundary conditions in all three directions. This resulted in a liquid slab of approximate width L separated by vacuum layers of approximate width $2L$. Some of the molecules were found to vaporize to the empty space to form a liquid–vapor interface on both sides of the liquid slab. In the simulations, the long-range electrostatic interactions were treated by using the three-dimensional Ewald method.⁴⁹ The real space part of the Ewald summation was calculated by using the minimum image convention, and the short-range Lennard-Jones interactions were calculated by using a spherical cutoff at distance $L/2$. We employed the quaternion formulation of the equations of rotational motion, and, for the integration over time, we adapted the leapfrog algorithm with a time step of 10^{-15} s (1 fs). MD runs of 500 ps were used to equilibrate each system in the bulk phase, and then the liquid–vapor interfacial systems in rectangular boxes were equilibrated for 500 ps. During the equilibration, the temperature of the simulation system was kept at 298 K through rescaling of the velocities. The simulations of the interfacial systems were then continued in a microcanonical ensemble for another 1 ns. The interfaces were found to be stable over the simulation time. The density, orientational profiles, surface tensions, hydrogen bonds, and the dynamical properties of the interfaces were calculated during the last production phase of the simulations.

3. Interfacial Structure and Surface Tension

We calculated the number density profile of water–methanol mixtures for various concentrations of methanol as a function of z by computing the average number of molecules in slabs of thickness $\Delta z = 0.05$ Å lying on either side of the central plane at $z = 0$, and the results are shown in Figure 1. It is seen that the methanol molecules have a higher propensity of staying in the interfacial region than water molecules which is in agreement with the experimental results.⁴⁶ The preferential presence of methanol molecules at interfaces is further discussed in the later part of this section.

The thickness of a liquid–vapor interface has been defined in the literature in different ways: By fitting the inhomogeneous density distribution to a hyperbolic tangent function^{50,51} or to an error function^{52,53} or by finding the distance over which the number density decreases from 90% to 10% of the bulk liquid density.^{54–56} The last definition is used in the present work to calculate the width of the liquid–vapor interfaces, and the results are shown in Figure 2 for varying mole fractions of methanol. The thickness of the interfaces is found to increase with increasing methanol mole fractions which can be attributed to weaker interactions and higher volatility of methanol molecules. For pure methanol, the present result of the interfacial thickness is very close to the result of ref 27 where a polarizable model of methanol was used. For water–methanol mixtures also, the present results of interfacial thickness agree rather well with the corresponding results of polarizable model calculations of ref 28. Note that the interfacial thicknesses of ref 28, which were obtained by fitting the density data to hyperbolic tangent

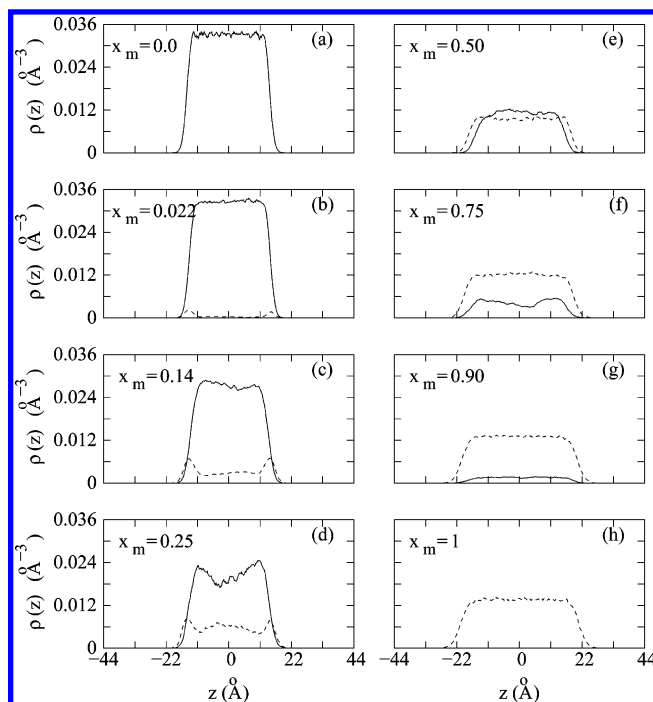


Figure 1. Number density profiles of liquid–vapor interfaces of water–methanol mixtures of varying composition. Solid curves representing water and dashed curves are for methanol.

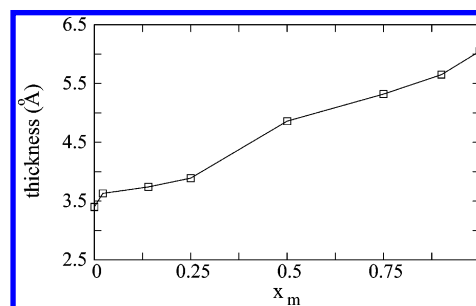


Figure 2. Interfacial thickness as a function of the mole fraction of methanol.

function, are to be multiplied by a factor of 2.1972^{27,50,51} to get the corresponding results of the 90–10 interface thickness which are then readily comparable to the results of the present study. We also note that the observed changes of the number densities at interfaces have contributions both from intrinsic changes of density profiles and also from broadening due to capillary wave fluctuations as allowed by the length and time scales of the present simulations.^{52,53,57,58} Thus, both intrinsic density changes and surface waves contribute to the lower number density in the interfacial regions. We can now make a more precise analysis of the enrichment of the interfaces by methanol or water molecules by plotting the mole fractions of water and methanol molecules at interfaces, defined as the 90–10 regions as described above, against that of the bulk liquid phases. Such plots are shown in Figure 3. It is clearly seen that the interfacial regions are enriched by methanol molecules. We note that the results of Figure 3 can be readily compared with the experimental results of Figure 6 of ref 46 where a similar surface enrichment by methanol molecules was found.

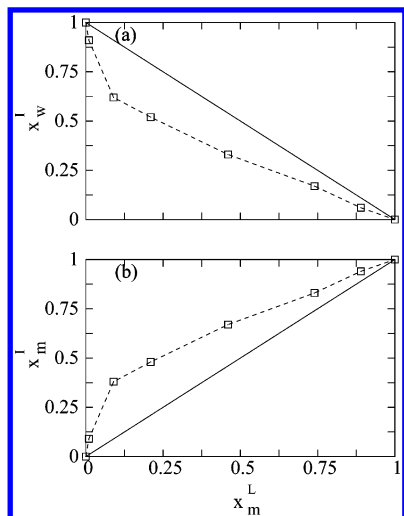


Figure 3. The variation of the mole fraction of (a) water and (b) methanol at interfaces with the mole fraction of methanol in the bulk liquid phases. The dashed lines are drawn only to connect the simulation results (squares). The solid lines correspond to the equal mole fractions of the interfacial and bulk liquid phases.

We note that, in Figure 3, x_m^L denotes the mole fraction of methanol in the bulk liquid region as obtained from the simulated densities. For low methanol mole fraction, the value of x_m^L is found to be slightly smaller than x_m which is the methanol mole fraction for the entire simulation system. This difference arises due to surface activity of methanol molecules and finite size of the simulation systems. For macroscopic systems, of course, this difference would be negligibly small.

We describe the orientation of a water molecule in terms of the angle θ that the molecular dipole vector makes with the surface normal along z -axis. We have calculated the orientational probability by dividing the angular region of $\cos\theta = -1$ to $+1$ into 60 bins of equal width and computing the average number of molecules found in a given bin. In Figure 4, we have shown the results of the normalized probability function $P(\cos\theta)$ as a function of $\cos\theta$ for both interfacial and bulk water molecules at various methanol concentrations. In the bulk phase, the probability function, as expected, is found to be uniform. Clearly, there is no preferred orientation of the water molecules in the bulk phase of the liquid slabs as one would expect. In the interfacial region, however, the probability function is nonuniform which shows an orientational structure of the interfacial molecules. For pure water, $P(\cos\theta)$ is maximum at around $\cos\theta = 0$ which means that water molecules at the interface prefer to orient with their dipoles parallel to the surface. One hydrogen atom projects into the liquid sides of the interface and other projects toward the vapor side of the interface. With an increasing methanol mole fraction, the angle θ increases which indicates that the dipole vector is tilted toward the liquid phase.

In Figure 5, we have shown the probability function of the orientation of the vector that bisects the C–O–H angle of a methanol molecule in the interfacial and bulk regions. The orientation of a methanol molecule is described by the

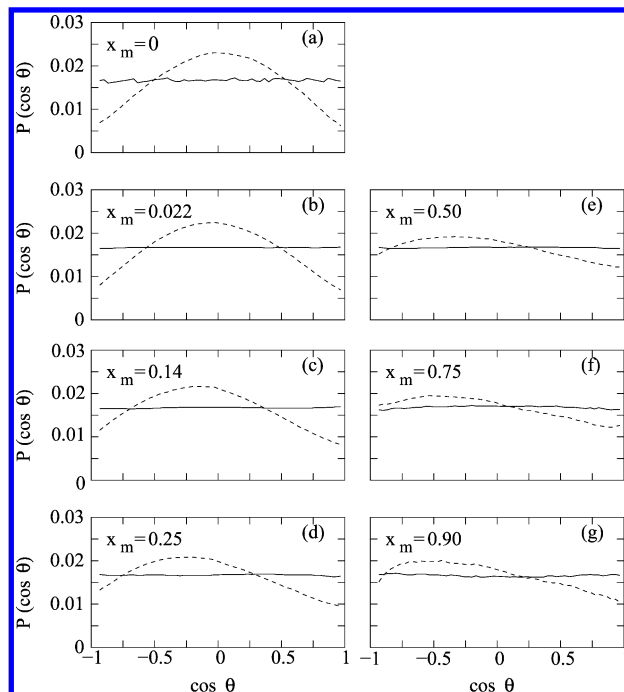


Figure 4. The probability function of the orientation of water dipole vectors in the interfacial (dashed) and bulk (solid) regions for different mole fractions of methanol. θ is the angle between the water dipole vector and the surface normal.

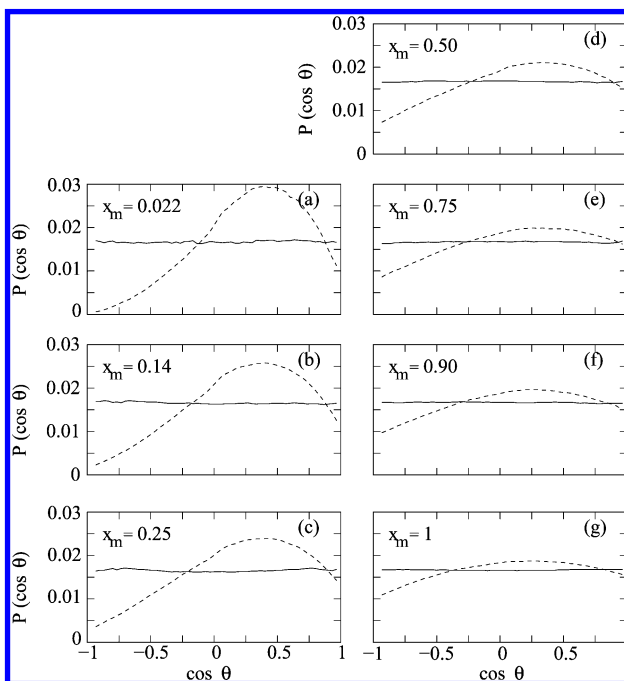


Figure 5. The probability function of the orientation of the bisector of the angle formed by the O–C and O–H bonds of a methanol molecule in the interfacial (dashed) and bulk (solid) regions for various methanol mole fraction. θ is the angle between the bisector and the surface normal.

angle θ that the above bisector vector makes with the surface normal. The orientational distribution of pure methanol is broad, and the maximum of $P(\cos\theta)$ appears at around $\cos\theta = 0.25$ which indicates that the angle between O–C vector and surface normal (θ') is about 21° . This means that the methyl group is projecting toward the vapor side and the

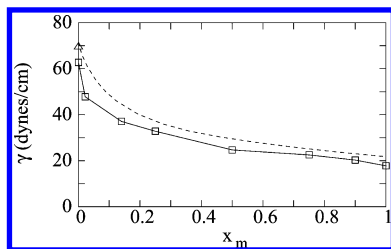


Figure 6. Surface tension vs mole fraction of methanol. Simulation data (open squares) are compared with experimental data (dashed curve) or refs 60 and 61. Diamond represents the simulated surface tension value of pure water with tail correction (ref 55).

hydroxyl hydrogen is pointed toward bulk liquid phases. This molecular orientation is also confirmed by a calculation of the orientation of the O–H vector of interfacial methanol molecules with respect to the surface normal. For example, for $x_m = 0.022$, the methanol O–H vector makes an angle of about 115° with the surface normal which clearly shows that the hydrogen is pointed inward. The ordering of surface methanol molecules increases with a decreasing methanol concentration. At very low concentration of methanol ($x_m = 0.022$) the value of the angle θ' is 5.7° which is consistent with the findings of experiments performed by Wolfrum, Graener, and Laubereau using the infrared-visible sum-frequency generation technique.²⁹ They reported that the value of θ' is less than 40° for pure methanol, and the polar order of methanol molecules at the surface of $\text{CH}_3\text{OH}-\text{H}_2\text{O}$ increases with a decreasing methanol concentration. At low methanol concentration ($x_m < 0.1$) the value of θ' was found to be approximately zero.²⁹

We calculated the surface tension by using the following virial expression which is obtained from the well-known Kirkwood–Buff theory⁵⁹

$$\gamma = \frac{1}{2A} \left\langle \sum_{i < j} \sum_{\alpha, \beta} \frac{\partial u_{\alpha\beta}}{\partial r_{\alpha\beta}} \frac{1}{r_{\alpha\beta}} (r_{ij} \cdot r_{\alpha\beta} - 3z_{ij}z_{\alpha\beta}) \right\rangle \quad (2)$$

where $u_{\alpha\beta}$ is the interaction energy between sites α and β of molecules i and j , r_{ij} and z_{ij} are the centers of mass distance and the distance along z direction between molecules i and j , and $r_{\alpha\beta}$ and $z_{\alpha\beta}$ are the corresponding distances between sites α and β . A is the total surface area which is equal to $2L^2$. We calculated the summations in the above expression at each MD step, and finally the averaging was done over the total number of MD steps that were run during the production phase of the simulations. The standard deviations of the surface tension data, which were calculated by using block averages over 100 ps, are about 4.5% of the average values reported. It is found that the surface tension decreases with an increase of methanol concentration. At all the methanol concentrations, our calculated values of the surface tension are somewhat lower than the experimental values. In Figure 6, we compare the calculated surface tension values, γ , for various mixtures with the available experimental results^{60,61} at 300 K. Although the calculated surface tension values are somewhat smaller than the experimental ones, the dependence on the composition of the mixtures is rather similar. Since the methanol molecules are strongly

adsorbed at the surface, a small amount of methanol has a rather large effect in reducing the surface tension. We also note that in the present study, the Lennard-Jones interactions are truncated at $L/2$ where L is the box length. Previous studies^{55,56,62} have shown that this potential truncation can underestimate the calculated surface tension to some extent. For example, the calculated surface tension of pure water at 298 K for SPC/E model was found to increase from about 62 to 70 upon inclusion of the tail corrections.⁵⁵ For the present systems also, we expect that similar tail corrections would improve the agreement between calculated and experimental results of the surface tension.

4. Hydrogen Bond Distribution at Interfaces

Following earlier studies on hydrogen bonds in water and aqueous solutions,^{63–67} we have used a set of geometric criteria to define the presence of a hydrogen bond between two molecules. Two water molecules are taken to be hydrogen bonded if their interoxygen distance is less than 3.5 \AA and simultaneously the hydrogen–oxygen distance is less than 2.45 \AA and the oxygen–oxygen–hydrogen angle is less than a cutoff value of 45° . A hydrogen bond between a water molecule and a methanol molecule exists if their interoxygen distance is less than 3.3 \AA and simultaneously the hydrogen–oxygen distance is less than 2.4 \AA . The cutoff value of the oxygen–oxygen–hydrogen angle is again 45° . A hydrogen bond between two methanol molecules occurs if their interoxygen distance is less than 3.5 \AA and simultaneously the hydrogen–oxygen distance is less than 2.6 \AA . Again, the cutoff value of the oxygen–oxygen–hydrogen angle is the same as for the water–water and water–methanol hydrogen bonds. The oxygen–oxygen and hydrogen–oxygen distances are determined from the positions of the first minimum of the corresponding radial distribution functions of the liquid mixtures. Following previous nomenclature in the context of water–water hydrogen bonds,⁶⁴ we have used a “less strict” definition of the hydrogen bonds in the present study. The quantities of interest are the percentages f_n of water or methanol molecules that engage in n hydrogen bonds and the average number of hydrogen bonds per molecule n_{HB} . Here we have calculated the above quantities for three types of hydrogen bonds: water–water (ww), water–methanol (wm), and methanol–methanol (mm).

In Figure 7, we have shown the variation of the number of hydrogen bonds per molecule with a change of methanol concentration in bulk liquid phases and also at interfaces. For pure water, in the bulk liquid phase, the majority of water molecules participate in four hydrogen bonds, whereas, in the liquid–vapor interfacial region, most of the molecules are found to have either three or two hydrogen bonds. The average number of hydrogen bonds per water molecule is also significantly smaller than that in the bulk liquid phase. This smaller number of hydrogen bonds at the vapor–water interfaces is likely due to the lower density and the presence of vapor (essentially vacuum) on one side of the liquid. Now with the increase of methanol concentration, the numbers of ww (water–water) and wm/m (water–methanol per methanol) hydrogen bonds decrease and that of wm/w (water–methanol per water) and mm (methanol–methanol) increases. We note that the average number of mm hydrogen

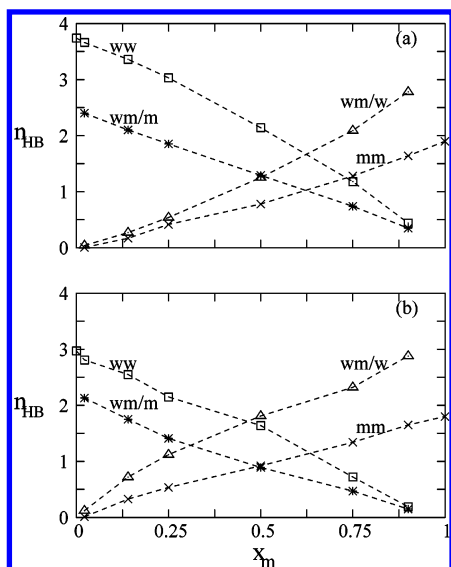


Figure 7. Variation of the number of hydrogen bonds per molecule at various methanol concentrations: (a) is for the bulk liquid region and (b) is for the interfacial region.

bonds in the interfacial region is higher than that in the bulk liquid up to $x_m = 0.90$ which clearly indicates that the methanol molecules are strongly adsorbed at the surface. Above $x_m = 0.90$ the average number of mm hydrogen bonds in the bulk liquid region is higher than that in the interfacial region. Figure 8 shows the fraction of molecules with n number of hydrogen bonds in bulk liquid and at the interfacial region for a 50:50 mixture of water and methanol. It is seen from Figure 8(b) that the number of wm hydrogen bonds per water molecule is somewhat higher in the interfacial region than that in the bulk liquid which can again be attributed to the higher population of methanol molecules in the surface region.

5. Diffusion and Orientational Relaxation of Interfacial Molecules

In this section, we report the single-particle dynamical properties of water and methanol molecules at the liquid–vapor interfaces that we have calculated in the present work. An important issue concerning the dynamics of an interface is as follows: How different the dynamics of the interface is compared to that of the corresponding bulk phases. The dynamical behavior of interfacial molecules is expected to be different from bulk molecules both translationally and rotationally. Also, the translational motion of molecules at the interface can be highly anisotropic in contrast to the bulk molecules which move in an isotropic environment. In view of this anisotropic aspect, we have separately calculated the perpendicular and parallel components of the translational diffusion. We have also calculated the dipole orientational relaxation of both the interfacial and bulk molecules.

We denote the α th component of velocity of a molecule by $v_\alpha(t)$ ($\alpha = x, y, z$), and its normalized autocorrelation function $C_{v,\alpha}(t)$ is defined by

$$C_{v,\alpha}(t) = \frac{\langle v_\alpha(t) v_\alpha(0) \rangle}{\langle v_\alpha^2 \rangle} \quad (3)$$

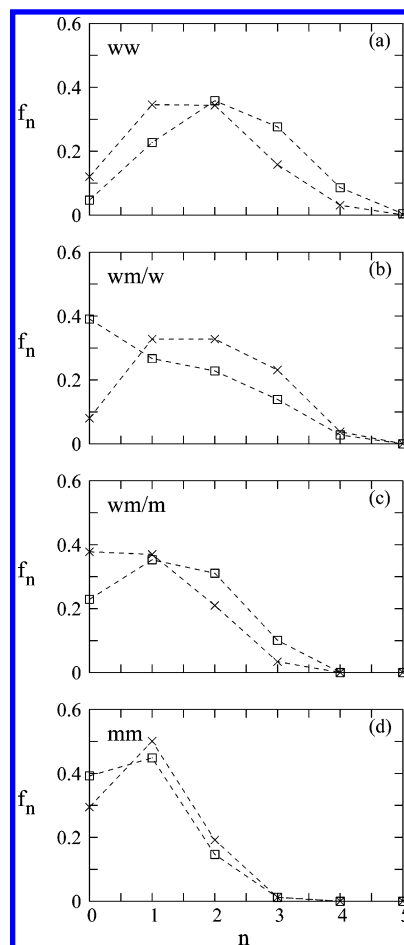


Figure 8. The fraction of molecules with n the number of hydrogen bonds in bulk liquid (open squares) and at the interfacial region (crosses) for a 50:50 mixture of water–methanol.

where $\langle \dots \rangle$ denotes an equilibrium ensemble average. In these calculations, the average of eq 3 is carried out over those molecules which are found in the interfacial region at time 0 and also at time t .

We have also calculated the diffusion coefficient D_α ($\alpha = x, y, z$) from the velocity–velocity autocorrelation function by using the following relation

$$D_\alpha = \frac{k_B T}{m} \int_0^\infty C_{v,\alpha}(t) dt \quad (4)$$

where m is the mass of a molecule and k_B is the Boltzmann constant. The anisotropic nature of the translational motion is clearly illustrated in Figure 9 where we have shown the diffusion coefficient values in the parallel (x) and perpendicular (z) direction of the interface, and the values are compared with their corresponding bulk liquid values at different mole fractions of methanol. We have also shown the experimental bulk diffusion coefficient values for both water and methanol molecules as reported in refs 8–11. At low concentration of methanol (upto $x_m = 0.25$) the diffusion coefficients of both water and methanol in the bulk liquid region decreases which indicates that there is significant interaction between the water and methanol molecules. Above $x_m = 0.25$ both $D^{\text{bulk}}(\text{H}_2\text{O})$ and $D^{\text{bulk}}(\text{CH}_3\text{OH})$ begin to increase. At low methanol concentrations, the methanol

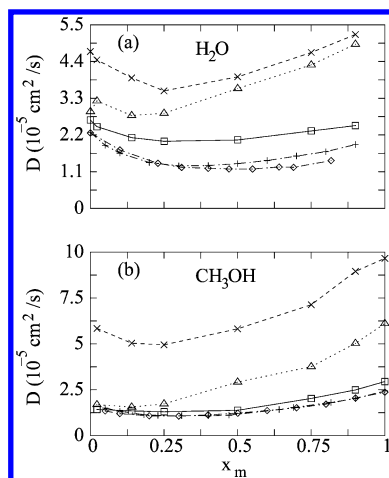


Figure 9. Diffusion coefficients as functions of methanol mole fraction: Open squares are for bulk liquids, open triangles are for diffusion coefficients at the interfacial z-direction, and crosses are for the interfacial x-direction, and plus signs and diamonds are experimental data from refs 8 and 10.

is rather strongly hydrated by a cage of water molecules^{13,17} leading to a retardation of their diffusion. At a high concentration of methanol, there are an insufficient number of water molecules present to form the hydration shells of all the methanol molecules. Thus, the relative importance of the strength of water–methanol interactions decreases, and, as a result, we observe an increase of the diffusion coefficients. The diffusion coefficients of both water and methanol molecules along the x -direction at the interface (parallel diffusion) follow the same trend as that of the corresponding bulk liquid values with the minimum of the diffusion coefficient values appearing at $x_m = 0.25$. For the perpendicular diffusion at interfaces, however, the minimum occurs at $x_m = 0.14$ for both water and methanol molecules. We note that, for pure water, the relative changes of the diffusion coefficients between the bulk and interfacial regions are qualitatively similar to the results obtained by Liu et al.⁶⁸ who used the method of survival probabilities to calculate the diffusion coefficients.

The rotational motion of a molecule at liquid–vapor interfaces is investigated by calculating the time dependence of the self-dipole correlation function

$$C_\mu(t) = \frac{\langle \mu(t) \cdot \mu(0) \rangle}{\langle \mu(0)^2 \rangle} \quad (5)$$

where $\mu(t)$ is the dipole vector of a molecule at time t . The results of $C_\mu(t)$ are shown in Figure 10 for both interfacial and bulk water and methanol molecules at varying methanol concentrations. It is seen that the orientational relaxation at the interface occurs at a faster rate than that in the bulk. We define the orientational relaxation time τ_μ as the time integral of the orientational correlation function

$$\tau_\mu = \int_0^\infty C_\mu(t) dt \quad (6)$$

where we have calculated the integral explicitly up to 4 ps by using the simulation data of $C_\mu(t)$, and the contribution of the tail part is obtained by using the fitted exponential

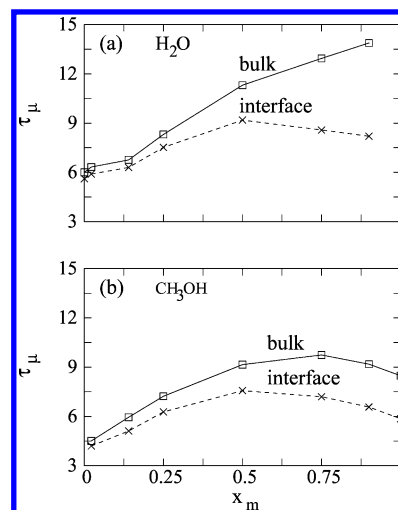


Figure 10. The dipole orientational relaxation times of (a) water and (b) methanol molecules in the interfacial (dashed line) and bulk regions (solid line) at various methanol mole fractions.

functions. The orientational relaxation time of interfacial molecules is found to be shorter than that of bulk molecules for all methanol mole fractions considered here. We note that the density of molecules is low in the interfacial region, and also the interfacial molecules have less number of hydrogen bonds and that they essentially do not have any solvation shell on the vapor side of the interface. Because of these reduced density, less number of hydrogen bonds and incomplete solvation effects, a molecule in the interfacial region experiences less rotational friction than that in the bulk phase leading to a faster rotational relaxation of interfacial molecules. We note that similar faster relaxation of the interfacial molecules than the bulk ones were also observed for liquid–vapor interfaces of pure water and aqueous ionic solutions.⁵⁵ Figure 10 shows that the rotational correlation times of methanol molecules has a maximum at $x_m = 0.50$ for the bulk liquid region and at $x_m = 0.25$ at the interface. For water molecules, the maximum appears at $x_m = 0.50$ for the interfacial region, but, for the bulk liquid region, the orientational correlation time of water increases monotonically with an increase of methanol concentration.

6. Dynamics of Hydrogen Bonds at Interfaces

The dynamics of hydrogen bonds in the interfacial and bulk regions are investigated by calculating the so-called continuous hydrogen bond time correlation functions^{64–67,69} and the average lifetimes of hydrogen bonds. We have calculated these dynamical properties for water–water, water–methanol, and methanol–methanol hydrogen bonds where both molecules are in the same region, interface or bulk, and also for inter-region hydrogen bonds where one molecule of the bonded pair is in the interface and the other is in the adjacent layer on the bulk side. For convenience, we denote the interfacial region as region I and the bulk region as region II.

To calculate the hydrogen bond dynamics, we first define two hydrogen bond population variables $h(t)$ and $H(t)$: $h(t)$

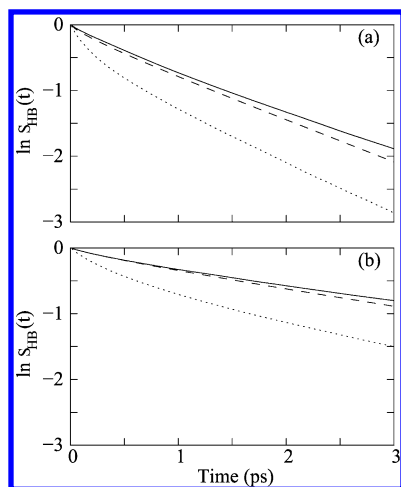


Figure 11. Time dependence of the correlation function $S_{HB}(t)$ for (a) pure water and (b) pure methanol. The solid, dashed, and dotted curves correspond to I–I, II–II, and I–II hydrogen bonds.

is unity when a particular tagged pair of water molecules is hydrogen bonded at time t , according to the adopted definition as described earlier and zero otherwise. The function $H(t)$ is unity if the tagged pair of water molecules remains continuously hydrogen bonded from $t = 0$ to time t , and it is zero otherwise. We define the continuous hydrogen bond time correlation function $S_{HB}(t)$ as^{61–64,66}

$$S_{HB}(t) = \langle h(0)H(t) \rangle / \langle h \rangle \quad (7)$$

where $\langle \dots \rangle$ denotes an average over all hydrogen bonds that are present at $t = 0$. Clearly, $S_{HB}(t)$ describes the probability that a water pair, which was hydrogen bonded at $t = 0$, remains continuously bonded up to time t . The time integral of this function describes the average time that a hydrogen bond survives after it is chosen at time $t = 0$. We denote the integral by τ_{HB} and call it the average hydrogen bond lifetime. We note, however, that since the hydrogen bonds are chosen randomly without keeping any condition on when they were created, the integral of $S_{HB}(t)$ should more appropriately be called the average persistence time of a randomly chosen hydrogen bond.⁶⁴

In Figure 11, we have shown the decay of $S_{HB}(t)$ for different regions of the liquid–vapor systems for pure water and pure methanol. The corresponding results for water–water, water–methanol, and methanol–methanol hydrogen bonds in water–methanol mixture with $x_m = 0.25$ are shown in Figure 12. The results of τ_{HB} for all the systems studied here are included in Tables 2–4. The relaxation of $S_{HB}(t)$ is found to be somewhat slower at liquid–vapor interfaces compared to the corresponding relaxation in the bulk phases. An insight into this different relaxation behavior of interfacial and bulk hydrogen bonds can be obtained from the energetics of these hydrogen bonds which are also included in Tables 2–4. The hydrogen bond energies are found to be most negative when both molecules are at the interface, whereas they are least negative when one molecule is at the interface and the other one is in the bulk liquid. Thus, although the number of hydrogen bonds in the liquid–vapor interfacial region is less as reported in Figures 7 and 8, the hydrogen

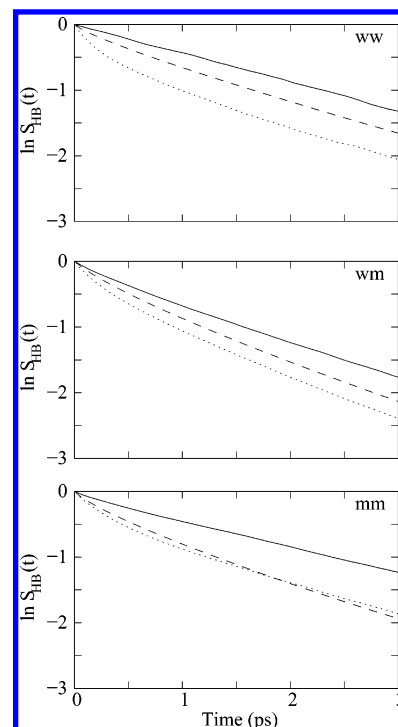


Figure 12. The time dependence of the correlation function $S_{HB}(t)$ for ww, wm, and mm hydrogen bonds for $x_m = 0.25$. Different curves are as in Figure 11.

Table 2. Lifetimes and the Energies of Water–Water (ww) Hydrogen Bonds for Different Mole Fractions of Methanol^a

x_m	region	τ_{HB}	E_{HB}
0.0	I–I	1.50	–19.74
	I–II	0.80	–18.65
	II–II	1.35	–18.72
0.25	I–I	2.28	–20.20
	I–II	1.15	–19.20
	II–II	1.68	–19.28
0.50	I–I	2.75	–20.46
	I–II	1.35	–19.63
	II–II	2.10	–19.83
0.75	I–I	3.13	–20.60
	I–II	1.43	–20.45
	II–II	2.70	–20.60

^a The relaxation times are expressed in units of ps, and the hydrogen bond energies are expressed in units of kJ/mol.

bonds in this region are found to be relatively stronger and hence live longer. Besides, as noted earlier,⁷⁰ the rate of relaxation of hydrogen bonds also depends on the number of adjacent but non-hydrogen-bonded water (or methanol) molecules. The higher the number of such non-hydrogen-bonded adjacent molecules, the faster would be the relaxation because these molecules can take a new hydrogen bond and thus help in breaking the original hydrogen bond. Since the number of such non-hydrogen-bonded adjacent molecules in the interfacial regions is smaller than that in the bulk liquids, the hydrogen bonds at the interfaces relax at a slower rate than those in the corresponding bulk liquid phases. An interesting dynamical behavior is found for the dynamics of those hydrogen bonds where one molecule of the bonded pair belongs to the interface (region I) and the second one

Table 3. Lifetimes and the Energies of Water–Methanol (wm) Hydrogen Bonds for Different Mole Fractions of Methanol^a

x_m	region	τ_{HB}	E_{HB}
0.25	I–I	1.60	–20.20
	I–II	1.05	–19.05
	II–II	1.25	–19.13
0.50	I–I	1.92	–20.80
	I–II	1.10	–19.54
	II–II	1.50	–19.64
0.75	I–I	2.22	–21.60
	I–II	1.28	–20.07
	II–II	1.80	–20.12

^a The relaxation times are expressed in units of ps, and the hydrogen bond energies are expressed in units of kJ/mol.

Table 4. Lifetimes and the Energies of Methanol–Methanol (mm) Hydrogen Bonds for Different Mole Fractions of Methanol^a

x_m	region	τ_{HB}	E_{HB}
0.25	I–I	2.36	–20.02
	I–II	1.30	–18.97
	II–II	1.40	–19.05
0.50	I–I	2.98	–20.24
	I–II	1.40	–19.40
	II–II	1.95	–19.55
0.75	I–I	4.13	–20.32
	I–II	1.52	–19.72
	II–II	2.50	–19.98
1.0	I–I	3.57	–20.27
	I–II	1.75	–19.92
	II–II	3.25	–20.10

^a The relaxation times are expressed in units of ps, and the hydrogen bond energies are expressed in units of kJ/mol.

to its adjacent region, i.e., region II. The dynamics of these inter-region hydrogen bonds are found to be faster than even those in the bulk phase. It is seen from Figures 7 and 8 that the hydrogen bond environment of different regions are different to some extent. The energetic data of Table 2 show that the energies of these inter-region or interenvironment hydrogen bonds are higher (least negative) than the corresponding intra-region hydrogen bonds for the bulk or interfacial zones. Thus, the hydrogen bonds that connect water molecules of two different regions or environments are found to be energetically weaker and hence relax at a faster rate than those belonging to a single region, either interface or the bulk. With an increase of methanol concentration, the average hydrogen bond lifetime (τ_{HB}) of ww and wm bonds increases in all three regions (I–I, I–II, and II–II), and this behavior is also supported by hydrogen bond energies. For mm hydrogen bonds, with increasing methanol mole fractions τ_{HB} increases in the II–II and I–II regions, but the τ_{HB} values at $x_m = 1.0$ are slightly lower than the corresponding values for $x_m = 0.75$ for the I–I region.

7. Conclusion

We have performed molecular dynamics simulations to investigate the various equilibrium and dynamical properties of liquid–vapor interfaces of water–methanol mixtures of

varying composition. Simulations are carried out at room temperature, and various interfacial properties that are calculated include density and orientational profiles, intrinsic width of the interfaces, surface tension, structure and dynamics of hydrogen bonds, molecular diffusion, and orientational relaxation of both water and methanol molecules.

It is found that the orientational distribution of the dipole vector of interfacial water molecules changes with a change of methanol concentration. The orientational ordering of methanol molecules at the surface of H_2O-CH_3OH is found to increase with a decrease of methanol concentration. At the interface, methanol molecules orient in such a way that the hydrophobic group seems to be oriented out of the surface plane which is in good agreement with the experimental results. The width of the interfaces, which is calculated by using the 90%–10% rule, is found to decrease, and the surface tension is found to increase with a decrease of the methanol mole fraction. Although the surface tension values calculated in the present study are somewhat lower compared to the experimental values, the trend of its variation with composition is very similar to the experimental results. The distribution of different types of hydrogen bonds (ww, wm, and mm) and the total number of hydrogen bonds per molecule are also calculated in both bulk liquid and interfacial regions.

The translational motion of water and methanol molecules is found to be highly anisotropic in the interfacial regions. The nonideal diffusive behavior with a variation of the methanol concentration is also found for interfacial diffusion where the minimum appears at a lower bulk methanol concentration because of the enrichment of the interfaces by methanol molecules. The rotational correlation times of methanol has a maximum at $x_m = 0.75$ at the bulk regions and $x_m = 0.50$ at the interface. For water, the orientational relaxation time increases monotonically with an increase of methanol concentration in the bulk region with no maximum. However, a maximum of the orientational relaxation time of interfacial water molecules is found at $x_m = 0.50$. We have also investigated the dynamics of water–water, water–methanol, and methanol–methanol hydrogen bonds at liquid–vapor interfaces and also in the bulk liquid phases. For all the systems, the relaxation of hydrogen bonds in the interfacial region is found to occur at a somewhat slower rate than that in bulk liquid. However, the dynamics of those hydrogen bonds which connect interfacial molecules to its adjacent layer on the bulk side is found to be faster than even the bulk hydrogen bonds. Correlations of these dynamical results with the energies of hydrogen bonds in different regions of the liquid–vapor systems are also explored. In addition, variation of the average lifetimes of different hydrogen bonds with composition of the water–methanol mixtures is also investigated.

In the present work, both water and methanol molecules are modeled as nonpolarizable molecules with fixed partial charges on various atomic sites. The solvent and solute molecules at liquid–vapor interfaces, however, encounter varying environments, and hence the degree of polarization of individual molecules can vary significantly across such

interfaces. Thus, the polarization effects can play an important role in determining the equilibrium and dynamical properties of liquid–vapor interfaces as has been shown in some of the recent theoretical studies on aqueous ionic solutions with large halide ions.^{71,72} In the context of the liquid–vapor interfaces of water–methanol systems, we note two recent studies^{27,28} where structural and thermodynamics aspects of such interfaces were examined by using polarizable models of water and methanol molecules. The inhomogeneous density and orientational profiles of the interfaces, including their dependence on the composition of the mixtures, for the polarizable models are found to be similar to the results of nonpolarizable models presented here. The thickness of the interfaces as found in these studies^{27,28} is also rather close to the results of the present study as discussed in section 3. The dynamical aspects of the liquid–vapor interfaces of water–methanol mixtures have not yet been investigated by using polarizable models. For the hydrogen bond dynamics at pure water surfaces, a recent study⁷⁰ has shown that many-body polarization effects can alter the relative time scales of relaxation of interfacial and bulk hydrogen bonds. Thus, it would be a worthwhile exercise to employ polarizable models to investigate the single-particle and hydrogen bond dynamical properties of liquid–vapor interfaces of water–methanol mixtures. There are several methods to account for the polarization effects in molecular dynamics simulations such as the fluctuating charge model,^{73,74} the model of dipoles on atomic sites,⁷⁵ the self-consistent reaction field method,⁷⁶ and the charge-on-spring model.^{77,78} We are currently developing polarizable models for different polyatomic molecules using the charge-on-spring model,^{77,78} and we hope to address the issue of many-body polarization effects on interfacial dynamics of water–methanol mixtures in a future publication. Also, in the present study, we have looked at the self-diffusion coefficients of bulk and interfacial molecules. It would also be worthwhile to study the mutual and distinct diffusion coefficients^{79–83} of water and methanol molecules in the bulk and interfacial regions. Such studies would reveal valuable information on the pair dynamics of these molecules which, in turn, would help us to investigate the tendency of these molecules to locally associate or demix, i.e., to create local heterogeneity, as one moves from the bulk to the surface regions.

Acknowledgment. One of the authors (A.C.) would like to thank Professor C. N. R. Rao, F.R.S., for helpful communications and enlightening discussions on surface enrichment in water–alcohol mixtures. The financial support from the Council of Scientific and Industrial Research (CSIR) and Department of Science and Technology (DST), Government of India, is gratefully acknowledged.

References

- (1) Narten, A. H.; Habenschuss, A. *J. Chem. Phys.* **1984**, *80*, 3387.
- (2) Yamaguchi, T.; Hidaka, K.; Soper, A. K. *Mol. Phys.* **1999**, *96*, 1159. Yamaguchi, T.; Hidaka, K.; Soper, A. K. *Mol. Phys.* **1999**, *97*, 603.
- (3) Morrone, J. A.; Tuckerman, M. E. *J. Chem. Phys.* **2002**, *117*, 4403.
- (4) Easteal, A. J.; Woolf, L. A. *J. Chem. Thermodyn.* **1985**, *17*, 69.
- (5) Easteal, A. J.; Woolf, L. A. *J. Chem. Thermodyn.* **1985**, *17*, 49.
- (6) Staveley, L. A. K.; Hart, K. R.; Tupman, W. I. *Discuss. Faraday Soc.* **1953**, *156*, 130.
- (7) Onori, G. *J. Chem. Phys.* **1987**, *87*, 1251.
- (8) Woolf, L. A. *Pure Appl. Chem.* **1985**, *57*, 1083.
- (9) Roux, A. H.; Desnoyers, J. E. *Proc. Indian Acad. Sci. (Chem. Sci.)* **1987**, *98*, 435.
- (10) Hawlicka, E. *Ber. Bunsen-Ges., Phys. Chem.* **1983**, *87*, 425.
- (11) Versmold, H. *Ber. Bunsen-Ges., Phys. Chem.* **1980**, *84*, 168.
- (12) Easteal, A. J.; Woolf, L. A. *J. Phys. Chem.* **1985**, *89*, 1066.
- (13) Jorgensen, W. L.; Madura, J. D. *J. Am. Chem. Soc.* **1983**, *105*, 1407.
- (14) Okazaki, S.; Nakanishi, K.; Touhara, H. *J. Chem. Phys.* **1983**, *78*, 454. Okazaki, S.; Touhara, H.; Nakanishi, K. *J. Chem. Phys.* **1984**, *81*, 890.
- (15) Bolis, G.; Corongiu, G.; Clementi, E. *Chem. Phys. Lett.* **1982**, *86*, 299.
- (16) Jorgensen, W. L. *J. Am. Chem. Soc.* **1980**, *102*, 543. Jorgensen, W. L. *J. Phys. Chem.* **1986**, *90*, 1276. Jorgensen, W. L.; Ibrahim, M. *J. Am. Chem. Soc.* **1982**, *104*, 373.
- (17) Soper, A. K.; Finney, J. L. *Phys. Rev. Lett.* **1993**, *71*, 4346.
- (18) Derlacki, Z. J.; Easteal, A. J.; Edge, A. V. J.; Woolf, L. A.; Roksandic, Z. *J. Phys. Chem.* **1985**, *89*, 5318.
- (19) Tanaka, H.; Gubbins, K. E. *J. Chem. Phys.* **1992**, *97*, 2626.
- (20) Skaf, M. S.; Ladanyi, B. M. *J. Chem. Phys.* **1995**, *102*, 6542.
- (21) Ferrario, M.; Haughney, M.; McDonald, I. R.; Klein, M. L. *J. Chem. Phys.* **1990**, *93*, 5156.
- (22) Day, T. J. F.; Patey, G. N. *J. Chem. Phys.* **1999**, *110*, 10937.
- (23) Wensink, E. J. W.; Hoffmann, A. C.; van Maaren, P. J.; van der Spoel, D. *J. Chem. Phys.* **2003**, *119*, 7308.
- (24) Morita, A. *Chem. Phys. Lett.* **2003**, *375*, 1.
- (25) Hawlicka, E.; Swiatla-Wojcik, D. *Phys. Chem. Chem. Phys.* **2000**, *2*, 3175.
- (26) Matsumoto, M.; Takaoka, Y.; Kataoka, Y. *J. Chem. Phys.* **1993**, *98*, 1464.
- (27) Patel, S.; Brooks, C. L., III *J. Chem. Phys.* **2005**, *122*, 24508.
- (28) Chang, T.-M.; Dang, L. X. *J. Phys. Chem. B* **2005**, *109*, 5759.
- (29) Wolfrum, K.; Graener, H.; Laubereau, A. *Chem. Phys. Lett.* **1993**, *213*, 41.
- (30) Huang, J. Y.; Wu, M. H. *Phys. Rev. E* **1994**, *50*, 3737.
- (31) Stanners, C. D.; Du, Q.; Chin, R.; Cremer, P.; Somorjai, G. A.; Shen, Y. R. *Chem. Phys. Lett.* **1995**, *232*, 407.
- (32) Eissenthal, K. B. *Chem. Rev.* **1996**, *96*, 1343 and references therein.
- (33) Du, Q.; Freysz, E.; Shen, Y. R. *Science* **1994**, *264*, 826. Du, Q.; Superfine, R.; Freysz, E.; Shen, Y. R. *Phys. Rev. Lett.* **1993**, *70*, 2313.

- (34) Goh, M. C.; Hicks, J. M.; Kemnitz, K.; Pinto, G. R.; Bhattacharyya, K.; Eienthal, K. B.; Heinz, T. F. *J. Phys. Chem.* **1988**, 92, 5074.
- (35) Sitzmann, E. V.; Eienthal, K. B. *J. Phys. Chem.* **1988**, 92, 4579.
- (36) Kemnitz, K.; Bhattacharyya, K.; Hicks, J. M.; Pinto, G. R.; Eienthal, K. B.; Heinz, T. F. *Chem. Phys. Lett.* **1986**, 131, 285.
- (37) Bhattacharyya, K.; Sitzmann, E. V.; Eienthal, K. B. *J. Chem. Phys.* **1987**, 87, 1442.
- (38) Petralli-Mallow, T.; Wong, T. M.; Byers, J. D.; Yee, H. I.; Hicks, J. M. *J. Phys. Chem.* **1993**, 97, 1383.
- (39) Superfine, R.; Huang, J. Y.; Shen, Y. R. *Opt. Lett.* **1990**, 15, 1276.
- (40) Conboy, J. C.; Daschbach, J. L.; Richmond, G. L. *J. Phys. Chem.* **1994**, 98, 9688.
- (41) Raising, T.; Stehlin, T.; Shen, Y. R.; Kim, M. W.; Valint, P., Jr. *J. Chem. Phys.* **1988**, 89, 3386.
- (42) Shi, X.; Borguet, E.; Tarnowski, A. N.; Eienthal, K. B. *Chem. Phys.* **1996**, 205, 167.
- (43) Wolfrum, K.; Lobau, J.; Laubereau, A. *Appl. Phys. A* **1994**, 59, 605.
- (44) Zimdars, D.; Eienthal, K. B. *J. Phys. Chem. B* **2001**, 105, 3993.
- (45) Zhang, D.; Gutow, J. H.; Eienthal, K. B.; Heinz, T. F. *J. Chem. Phys.* **1993**, 98, 5099.
- (46) Raina, G.; Kulkarni, G. U.; Rao, C. N. R. *J. Phys. Chem. A* **2001**, 105, 10204.
- (47) Haughney, M.; Ferrario, M.; McDonald, I. R. *J. Phys. Chem.* **1987**, 91, 4934. Haughney, M.; Ferrario, M.; McDonald, I. R. *Mol. Phys.* **1986**, 58, 849.
- (48) Berendsen, H. J. C.; Grigera, J. R.; Straatsma, T. P. *J. Phys. Chem.* **1987**, 91, 6269.
- (49) Allen, M. P.; Tildesley, D. J. *Computer Simulation of Liquids*; Oxford, 1987.
- (50) Chapela, G. A.; Saville, G.; Thompson, S. M.; Rowlinson, J. S. *J. Chem. Soc., Faraday Trans. 2* **1977**, 8, 133.
- (51) Rowlinson, J. S.; Widom, B. *Molecular theory of capillarity*; Clarendon: Oxford, 1982.
- (52) Sides, S. W.; Grest, G. S.; Lacasse, M.-D. *Phys. Rev. E* **1999**, 60, 6708.
- (53) Senapati, S.; Berkowitz, M. L. *Phys. Rev. Lett.* **2001**, 87, 176101.
- (54) Taylor, R. S.; Dang, L. X.; Garrett, B. C. *J. Phys. Chem.* **1996**, 100, 11720.
- (55) Paul, S.; Chandra, A. *Chem. Phys. Lett.* **2003**, 373, 87.
- (56) Alejandre, J.; Tildesley, D. J.; Chapela, G. A. *J. Chem. Phys.* **1995**, 102, 4574.
- (57) Lacasse, M.-D.; Grest, G. S.; Levine, A. J. *Phys. Rev. Lett.* **1998**, 80, 309.
- (58) Werner, A.; Schmid, F.; Müller, M.; Binder, K. *Phys. Rev. E* **1999**, 59, 728.
- (59) Kirkwood, J. G.; Buff, F. P. *J. Chem. Phys.* **1949**, 17, 338.
- (60) *CRC Handbook of Chemistry and Physics*, 72nd ed.; Lide, D. R., et al., Eds.; CRC: Boston, 1991.
- (61) *International Critical Tables of Numerical Data, Physics, Chemistry and Technology*; Washburn, E. W., Ed.; McGraw-Hill Book Company, Inc.: New York and London, 1928; Vol. 4.
- (62) Mecke, M.; Winkelmann, J.; Fischer, J. *J. Chem. Phys.* **1999**, 110, 1188.
- (63) Luzar, A.; Chandler, D. *Nature (London)* **1996**, 379, 53. Luzar, A.; Chandler, D. *Phys. Rev. Lett.* **1996**, 76, 928.
- (64) Luzar, A. *J. Chem. Phys.* **2000**, 113, 10663.
- (65) Chandra, A. *Phys. Rev. Lett.* **2000**, 85, 768. Chandra, A. *J. Phys. Chem. B* **2003**, 107, 3899.
- (66) Balasubramanian, S.; Pal, S.; Bagchi, B. *Phys. Rev. Lett.* **2002**, 89, 115505.
- (67) Paul, S.; Chandra, A. *Chem. Phys. Lett.* **2004**, 386, 218.
- (68) Liu, P.; Harder E.; Berne, B. J. *J. Phys. Chem. B* **2004**, 108, 6595.
- (69) Rapaport, D. *Mol. Phys.* **1983**, 50, 1151.
- (70) Liu, P.; Harder E.; Berne, B. J. *J. Phys. Chem. B* **2005**, 109, 2949.
- (71) Jungwirth, P.; Tobias, D. J. *J. Phys. Chem. B* **2001**, 105, 10468.
- (72) Jungwirth, P.; Tobias, D. J. *J. Phys. Chem. B* **2002**, 106, 6361.
- (73) Rick, S. W.; Stuart, S. J.; Berne, B. J. *J. Chem. Phys.* **1994**, 101, 6141.
- (74) Rick, S. W. *J. Chem. Phys.* **2001**, 114, 2276.
- (75) Koneshan, S.; Rasaiah J. C.; Dang, L. X. *J. Chem. Phys.* **2001**, 114, 7544.
- (76) Luque, F. J.; Bofill, J. M.; Orozco, M. *J. Chem. Phys.* **1995**, 103, 10183.
- (77) Straatsma, T. P.; McCammon, J. A. *Mol. Simul.* **1990**, 5, 181.
- (78) Yu, H.; Hansson, T.; van Gunsteren, W. F. *J. Chem. Phys.* **2003**, 118, 221.
- (79) Jacucci, G.; McDonald, I. R. *Physica A (Amsterdam)* **1975**, 80, 607.
- (80) Schoen, M.; Hoheisel, C. *Mol. Phys.* **1984**, 52, 33.
- (81) Ali, S. M.; Samanta, A.; Ghosh, S. K. *J. Chem. Phys.* **2001**, 114, 10419.
- (82) Chowdhuri, S.; Chandra, A. *Phys. Rev. E* **2002**, 66, 41203.
- (83) Kamala, C. R.; Ayappa, K. G.; Yashonath, S. *J. Phys. Chem. B* **2004**, 108, 4411.